

Gating Reaction Mechanisms for NMDA Receptor Channels

Yu Zhou and Anthony Auerbach

Center for Single Molecule Biophysics and Department of Physiology and Biophysics, State University of New York, Buffalo, New York 14214

NMDA receptors (NMDARs) mediate the slow component of excitatory transmission in the CNS and play key roles in synaptic plasticity and excitotoxicity. We investigated the gating reaction mechanism of fully liganded NR1/NR2A recombinant NMDARs (expressed in *Xenopus* oocytes) by fitting all possible three-closed/two-open-state, noncyclic kinetic schemes to currents elicited by saturating concentrations of glutamate plus glycine. The adequacy of each scheme was assessed by maximum likelihood values and autocorrelation coefficients of single-channel currents, as well as by the predicted time courses of transient macroscopic currents. Two schemes provided the best description for NMDAR gating at both the single-channel and macroscopic levels. These two schemes had coupled open states, only one gateway between the closed and open aggregates, and at least two preopening closed states. These two models could be condensed into a cyclic reaction mechanism. Using a linear reaction scheme, the overall “gating” rates (from the initial stable closed state to the final stable open state) are 177 and 4.4 s⁻¹.

Key words: channel; kinetics; oocyte; glutamate receptor; glutamate; NMDA receptor

Introduction

NMDA receptors (NMDARs) are glutamate-gated ion channels that are Ca²⁺ permeable and experience voltage-dependent block by Mg²⁺ (Mayer et al., 1984; Nowak et al., 1984; Wollmuth and Sakmann, 1998; Wollmuth et al., 1998). These special properties, and their slow activation and deactivation rates, make NMDARs an important contributor to long-term synaptic plasticity and excitotoxicity (Hollmann and Heinemann, 1994; Dingledine et al., 1999). NMDARs are typically composed of two NR1 and two NR2 subunits that bind glycine and glutamate, respectively (Benveniste and Mayer, 1991a; Clements et al., 1992; Behe et al., 1995; Rosenmund et al., 1998). Structural studies indicate that the binding of agonists causes a conformational change in the S1–S2 binding site domains of the protein (Sun et al., 2002; Furukawa and Gouaux, 2003), which is likely to be an early conformational event that leads to the isomerization of the ion channel domain from an ion-impermeable [“closed” (C)] conformation to an ion-permeable [“open” (O)] conformation. However, the details of the molecular events that constitute the global conformational change in the protein (“gating”) remain unknown. Kinetic models are useful in this regard, because they serve to encode the energy landscape for dynamic changes in protein structure. Furthermore, such models have predicative value and can be used to both interpret and forecast the behavior of NMDARs at synapses (Popescu and Auerbach, 2004; Popescu et al., 2004).

Kinetic models of NMDAR activity that have been derived by fitting macroscopic currents have focused mainly on agonist-

binding steps (Benveniste and Mayer, 1991a; Clements et al., 1992; Lester and Jahr, 1992). In these schemes, the gating conformational change is usually represented simply as a single-step reaction. Although these models can explain the time course of macroscopic NMDAR currents, they fail to describe the complex kinetics of single-channel NMDAR currents (Gibb and Colquhoun, 1991, 1992; Stern et al., 1992). Recently, more complex models for fully liganded NMDAR gating have been proposed (Banke and Traynelis, 2003; Popescu and Auerbach, 2003). In the Banke and Traynelis (BT) model (Banke and Traynelis, 2003), fully liganded (NR1/NR2B) NMDARs can occupy four closed and only one open state. Based on the observation that partial agonists of each of the two classes of binding sites only change one component of the closed-time distribution, Banke and Traynelis proposed a gating mechanism in which the NR1 and NR2 subunit pairs isomerize independently, followed by an additional conformational change that changes the conductance of the pore. In the model of Popescu and Auerbach (2003), fully liganded (NR1/NR2A) NMDARs can adopt multiple activation modes, each of which has three closed and two coupled open states. Although these two models are similar, it remains important to define more precisely a kinetic scheme for NMDAR gating that can be related to specific structural changes in the protein, as well as be used to make predictions about the time course and amplitudes of synaptic currents (Popescu et al., 2004).

Here, we present a statistical analysis of single-channel and macroscopic currents induced by saturating agonists from NR1a/NR2A NMDARs expressed in *Xenopus* oocytes. All possible three-closed/two-open (3C2O) noncyclic schemes were fitted to quantitatively assess their abilities to describe fully liganded NMDAR gating. The two optimal schemes have coupled open states, the first of which is preceded by at least two closed states, and only one entry/exit state between the closed and open aggregates. These schemes can be combined into a cyclic model in which a closed, fully liganded NMDAR can choose between two

Received April 14, 2005; revised July 5, 2005; accepted July 5, 2005.

This work was supported by National Institutes of Health Grant 5R01NS036554-07 to A.A. We thank M. Teeling for technical assistance and P. Seeburg and T. Kuner for the NMDA receptor subunit cDNAs.

Correspondence should be addressed to Anthony Auerbach, Department of Physiology and Biophysics, State University of New York, 324 Cary Hall, Buffalo, NY 14214. E-mail: auerbach@buffalo.edu.

DOI:10.1523/JNEUROSCI.1471-05.2005

Copyright © 2005 Society for Neuroscience 0270-6474/05/257914-10\$15.00/0

preopening conformational pathways before reaching an ion-conducting state.

Materials and Methods

Expression of cRNA in oocytes

RNA was transcribed *in vitro* from cDNA by standard methods. To express NMDARs, the RNAs of rat NR1a and NR2A were coinjected at a nominal ratio of 1:1 in *Xenopus* oocytes. Patch-clamp recordings were made 3–10 d after injection. A detailed description of the molecular biology and expression protocols has been described previously (Premkumar and Auerbach, 1996).

Electrophysiological recording

Single-channel and macroscopic currents were recorded from outside-out or cell-attached patches (Hamill et al., 1981). The temperature was 23–25°C. Agonists were contained in the pipette solution (cell-attached patches) or applied to outside-out patches by using a fast perfusion system. The perfusion pipette was pulled from double-barreled glass tubing (tip diameter, 200 μm) and attached to a bimorph actuator (model QP22B; ACX, Cambridge, MA) using epoxy resin. External solutions were delivered to each of the two barrels by using air pressure. The actuator was controlled by QUB software (<http://www.qub.buffalo.edu>) to move the solution interface across the tip of patch pipette. The command voltage pulses were low-pass filtered at 150 Hz. The actual solution-exchanging rate was routinely measured on the same patch pipette at the end of each recording by open-tip response (Jonas, 1995). The 10–90% rise time of this system was $\sim 200 \mu\text{s}$ (see Fig. 4a, inset).

Patch pipettes were pulled from borosilicate capillary glass (Sutter Instruments, Novato, CA), coated with Sylgard 184 (Dow Corning, Midland, MI), and fire-polished before recording. The pipette resistance ranged from 0.5 to 2 M Ω for macropatches and 10 to 20 Ω for single-channel recording. The pipette solution contained the following (in mM): 100 Na gluconate, 10 NaCl, 10 BAPTA, 10 HEPES, 2 K₂ATP, and 0.25 GTP. The pH of the pipette solution was adjusted to 7.3 by using NaOH. The extracellular solution contained the following (in mM): 100 NaCl, 2 KCl, 1 EDTA (to eliminate Mg²⁺ block), 10 N-(2-hydroxyethyl)-piperazine-N[E-(4-butanedisulfonic acid)], pH adjusted to 8 (to minimize proton inhibition) by using NaOH. All chemicals were purchased from Sigma (St. Louis, MO) or Aldrich (Milwaukee, WI). Currents were amplified (PC-505B; Warner Instruments, Hamden, CT), low-pass filtered at 20 kHz (eight-pole Bessel; LPF-8; Warner Instruments), and digitized at 40 kHz directly to a hard disk using a MIO-16E digital board (National Instruments, Austin, TX).

Data analysis

Conductance level detection and amplitude histograms. The conductance levels of NMDARs were detected by variance–mean analysis (Patlak, 1988). A window of length N sampling points was centered over each sample of current, and the variance (σ^2) and mean amplitude (I) of the current within the window were calculated. The window was advanced by one sample, and the pair of σ^2 and I values was again calculated, with this process repeated for the entire record. If the sliding window covers more than one conductance level, the variance will increase. Changes in conductance were identified by the transitions in the variance points relative to that of the baseline (σ_b^2). This analysis was performed by a program written in OriginC language (OriginLab, Northampton, MA).

Simulation, idealization, and maximum likelihood fitting. QUB software was used for simulation, idealization, and modeling of single-channel currents. Data were corrected for slow and nonperiodic baseline drifts using manually specified piecewise linear functions and then idealized by a segmental k -means method (Qin, 2004). Clusters of single-channel current openings were chosen by excluding the longest closed events (desensitization) by invoking a critical shut time (t_{crit}) that was based on an equal number of misclassified events (Magleby and Pallotta, 1983; Clapham and Neher, 1984). Bursts from patches having only one active channel were concatenated as a continuous “active-time” record. To test for kinetic homogeneity, this record was divided into 1 s segments and idealized by using a two-state ($C \rightleftharpoons O$) model to calculate a segment mean open and closed time. The kinetic modeling was based on clusters

rather than the segmented record. The currents were idealized using the segmental k -means (SKM) algorithm and the rate constants for a given model were estimated by using a full maximum likelihood approach (Qin et al., 1996; Qin, 2004) after imposing a “dead time” of two to three sampling intervals (50–75 μs). The dwell times given by the SKM method are integer multiples of the sampling interval (25 μs).

Correlation analysis. To help ascertain the connectivity of the states in the model, two-dimensional (2D) dependency plot analysis (Magleby and Song, 1992) and open–open, closed–closed, and open–closed autocorrelation analyses (Fredkin et al., 1985; Labarca et al., 1985) were performed on idealized single-channel data without correcting for missed events. The autocorrelation coefficient for two intervals T_1 and T_2 in an idealized single-channel current is as follows:

$$\rho(T_1, T_2) = \frac{\text{cov}(T_1, T_2)}{\sqrt{\text{var}(T_1)\text{var}(T_2)}} = \frac{E(T_1, T_2) - \mu_1\mu_2}{\sqrt{[E(T_1^2) - \mu_1^2][E(T_2^2) - \mu_2^2]}} \quad (1)$$

where the means are $\mu_1 = E(T_1)$ and $\mu_2 = E(T_2)$.

Thus, the autocorrelation coefficient between an open (or closed) interval T and the k th open (or closed) interval T' behind is as follows:

$$\rho(k) = \frac{[E(TT') - \mu^2]}{\sigma^2} \quad (2)$$

where μ is the mean and σ^2 is the variance of open (or closed) dwell times in the recording. The autocorrelation coefficient between an open interval T_O and the k th closed interval T_C behind is as follows:

$$\rho(k) = \frac{[E(T_O T_C) - \mu_{\text{open}}\mu_{\text{closed}}]}{\sqrt{\sigma_{\text{open}}^2\sigma_{\text{closed}}^2}} \quad (3)$$

According to theorem 5.1 of Fredkin et al. (1985), the autocorrelation coefficient decays geometrically with increasing lag k if there is more than one entry/exit state between open and closed aggregates. The correlation coefficients were used to test the activation mechanisms of ACh receptor in adult frog muscle (Colquhoun and Sakmann, 1985).

The 2D dependency, $d(t_O, t_S)$, is as follows:

$$d(t_O, t_S) = \frac{f(t_O, t_S) - f'(t_O, t_S)}{f(t_O, t_S)} \quad (4)$$

where $f(t_O, t_S)$ is the observed 2D probability density function and $f'(t_O, t_S) = f_O(t_O)f_S(t_S)$ is the expected 2D probability density function if there is no dependence between paired open and closed intervals. To create the 2D dwell-time distribution of adjacent open and shut intervals, the logs of the durations of each open interval and the following closed interval were used to locate a bin on the x – y plane, with the z -axis indicating the square root of the number of interval pairs in each bin (Sigworth and Sine, 1987). The 2D dwell-time distributions were then smoothed by using the weighted average value of nine bins in a 3×3 array with three bins per side moving through the x – y plane (Song and Magleby, 1994). The weighted average is calculated as follows:

$$\bar{a} = \frac{0.707(a_{11} + a_{13} + a_{31} + a_{33}) + (a_{12} + a_{21} + a_{22} + a_{23} + a_{32})}{7.828} \quad (5)$$

where a_{11} through a_{33} are the elements in the moving array:

$$\begin{array}{ccc} a_{11} & a_{12} & a_{13} \\ a_{21} & a_{22} & a_{23} \\ a_{31} & a_{32} & a_{33} \end{array} \quad (6)$$

Programs written in OriginC language were used for the correlation analyses and 2D dependency plots. Autocorrelation coefficients of open–open, closed–closed, and open–closed interval pairs predicted by kinetic models (Colquhoun and Hawkes, 1987) were calculated by using a worksheet written in Maple 7 (Waterloo Maple, Waterloo, Ontario, Canada).

Macroscopic current analysis. Normalized macroscopic currents were computed from each kinetic model (Colquhoun and Hawkes, 1995a,b) by using a Maple 7 worksheet. The 5–95% rising and decay phases of the computed and experimentally recorded macroscopic currents were compared by eye and by calculating the deviation of simulated response from experimental current by using the following function:

$$d = \sum \frac{(\text{recorded} - \text{simulated})^2}{|\text{simulated}|}. \quad (7)$$

All data are expressed as the mean \pm SD.

Results

Single-channel activity of NMDARs

Under physiological conditions, the kinetic behavior of NMDARs at the single-channel level is difficult to interpret because of the binding of multiple agonists and inhibition by several types of ions, including protons and Mg^{2+} . To simplify matters, we used supermaximal concentrations of glutamate and glycine (to saturate the binding sites at steady state or to maximally accelerate binding after a concentration jump) and high pH, divalent cation-free extracellular solutions (to reduce or eliminate ion inhibition). Figure 1*a* shows single-channel currents from an outside-out patch exposed to 1 mM glutamate and 100 μM glycine. Figure 1*b* shows the corresponding variance–mean amplitude histogram fitted by the sum of two Gaussian components, one for the ion-conductive level and the other for the nonconductive level. Although brief superconductance- and subconductance-level events occasionally appeared (Fig. 1*a*, bottom traces), they were rare and were not analyzed further. The mean conductance of NMDARs measured from six patches was 73.2 ± 2.3 pS, which is $\sim 40\%$ greater than in physiological solutions containing 1 mM CaCl_2 (Stern et al., 1992, 1994).

The activation of NMDARs at saturating agonist concentrations occurs as groups of closely spaced openings (“clusters”) separated by sojourns in long-lived nonconducting states that reflect desensitization (Sakmann et al., 1980; Banke and Traynelis, 2003; Popescu and Auerbach, 2003). The desensitized sojourns were excluded from our analyses after invoking a t_{crit} and only the intracluster currents were considered to be part of the overall gating isomerization event. NR1/NR2A NMDARs expressed in human embryonic kidney (HEK) cells [and cotransfected with green fluorescent protein (GFP)] adopt at least three activity patterns (“modes”) that have characteristic mean open times (Popescu and Auerbach, 2003). However, in our experiments, these same subunits (expressed in oocytes by mRNA injection) gave rise to NMDARs that were kinetically homogeneous. As shown in Figure 1*c*, the mean open and closed times for each second of “active time” were, in general, constant throughout the recording period (>20 min). Similar results were obtained from data recorded from cell-attached patches (Fig. 1*c*, inset).

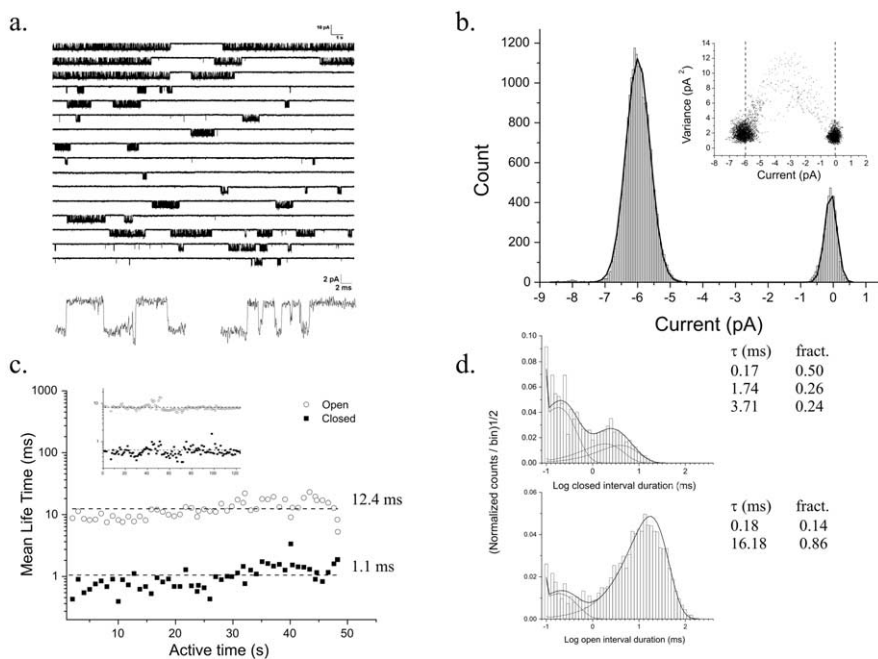


Figure 1. Single-channel activity of NMDARs elicited by 1 mM glutamate and 100 μM glycine in the presence of 1 mM EDTA. *a*, Continuous record from an outside-out patch at -80 mV. Occasional alternative conductance levels are displayed on an expanded time scale below. *b*, Amplitude histogram constructed from activation bursts and the corresponding mean–variance analysis (inset, 10-sample sliding window). There is primarily one conducting amplitude level with a mean of 5.99 pA. *c*, The mean closed and open durations for each second of active time are stable. An interval duration stability analysis from a cell-attached patch is shown (inset). *d*, Duration distributions of intracluster closed (top) and open (bottom) intervals. Mean lifetimes and relative areas of each exponential component are shown (right). fract., Fraction.

Table 1. Time constants and fractional amplitudes of closed and open intervals within clusters

Patch No.	τ_{c1} [ms (%)]	τ_{c2} [ms (%)]	τ_{c3} [ms (%)]	τ_{o1} [ms (%)]	τ_{o2} [ms (%)]
12170303	0.17 (50)	1.74 (26)	3.71 (24)	0.18 (14)	16.18 (86)
12170304	0.14 (54)	0.99 (12)	3.16 (34)	0.16 (11)	14.10 (89)
12170305	0.17 (50)	1.48 (18)	3.85 (32)	0.18 (12)	11.54 (88)
12170306	0.16 (53)	1.45 (12)	3.41 (35)	0.19 (9)	12.62 (91)

Distributions of intracluster closed and open intervals recorded from outside-out patches were best fitted by three and two exponential components, respectively (Fig. 1*d*, Table 1). The three closed components had mean time constants (relative areas) of 0.16 ± 0.014 ms ($52 \pm 2.1\%$), 1.42 ± 0.31 ms ($17 \pm 6.6\%$), and 3.53 ± 0.31 ms ($31 \pm 5.0\%$). The corresponding values for the two open components were 0.18 ± 0.012 ms ($12 \pm 2.1\%$) and 13.61 ± 2.01 ms ($88 \pm 2.1\%$) ($n = 4$). These distributions are similar to those of M-mode NR1a/NR2A NMDARs expressed in HEK cells (Popescu and Auerbach, 2003). However, the mean time constants of the two briefest closed components were longer than those recorded in the presence of low concentrations of agonist and divalent cations (Stern et al., 1994; Wyllie et al., 1998). It is possible that this difference is attributable to the absence of fast Mg^{2+} block in our divalent cation-free solution.

The interval duration distributions of intracluster, single-channel events recorded from cell-attached patches were also well fitted by three closed and two open components. The mean time constants (relative areas) of three closed components were 0.075 ± 0.021 ms ($50 \pm 1\%$), 0.48 ± 0.1 ms ($28 \pm 7\%$), and 4.29 ± 0.14 ms ($22 \pm 7\%$). For the two open components, these values were 0.42 ± 0.23 ms ($14 \pm 9\%$) and 10.63 ± 4.41 ms ($86 \pm 12\%$) ($n = 3$). The distributions from cell-attached and outside-out recordings were similar. The kinetic studies described below

were mainly derived from analyses of currents from outside-out patches.

Kinetic modeling of single-channel data

The duration distributions of intraburst events indicate that a parsimonious activation scheme for NMDARs must have three closed and two open states (Colquhoun and Hawkes, 1981, 1982). These five states can be arranged to constitute 15 noncyclic kinetic models, six of which have coupled open states (Table 2). All 15 models were fitted to the intracuster interval durations (four patches) by using a full maximum likelihood approach, with all eight rate constants allowed to vary. Seven of these models gave an equivalent maximum log likelihood (LL) value that was higher (>10 LL units) than those from the other eight models (Table 3). The models having coupled open states always gave

higher log likelihood values than those with uncoupled open states.

The seven best models can be further classified by their connectivities. In models 4, 5, and 7, there are two entry/exit states between the open and closed aggregates (O_1 and O_2), whereas in models 1, 8, 11, and 12, there is only one (O_1). A model with connectivity >1 predicts the existence of an autocorrelation between open, closed, or open–closed interval pairs in single-channel data (Fredkin et al., 1985; Colquhoun and Hawkes, 1987).

Autocorrelation coefficients predicted by models 4, 5, and 7 were calculated by a method provided by Colquhoun and Hawkes (1987). As shown in Figure 2a, model 4 predicts a negative correlation between open–closed pairs, a positive (but smaller) correlation between open–open pairs and a weak, positive correlation between closed–closed pairs. Similar predictions

hold for the other two models having a connectivity of 2 (models 5 and 7). The open–closed correlation coefficients for lag $k = 1$ predicted by models 4, 5, and 7 were approximately -0.03 , which could be readily detected in data simulated from these models when the number of intervals was >9000 (Fig. 2b). However, there were no significant autocorrelations between open–open, closed–closed, or open–closed interval pairs in the experimental NMDAR currents. As illustrated in Figure 2d, all three types of correlation coefficients in an activation cluster recorded from an outside-out patch were normally distributed around zero. Similar results were obtained from several long activation clusters having >9000 intervals, from cell-attached patches (Fig. 2d, inset). Moreover, the 2D dependency plots of the experimental current intervals did not show any significant excess or deficit in open–closed pairs within clusters (Fig. 2c). The above correlation analyses and dependency plots were not corrected for missed events. However, the consequence of this omission may not be crucial, because no correlations were detected in the experimental data. Thus, the results indicate that the activation model for NMDAR should have only one entry/exit state through which the open and closed aggregates communicate. Based on these analyses, four models (1, 8, 11, and 12) were selected for additional consideration.

In theory, the full maximum likelihood analysis should take into account all of the information in a single-channel record, including dependency between successive events in the record (Colquhoun and Hawkes, 1995a). However, spurious events generated by noise, errors in detection, and rare channel behaviors limit the usefulness of the LL discriminator. Dependency and autocorrelation analyses are valuable complements to maximum like-

Table 2. Noncyclic models having three closed and two open states

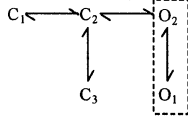
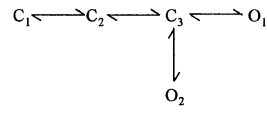
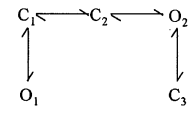
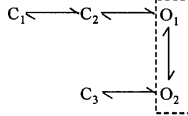
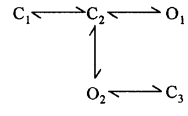
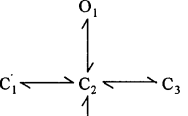
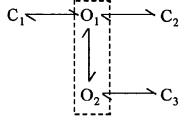
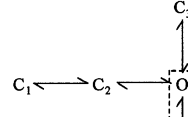
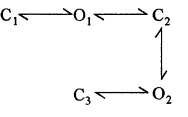
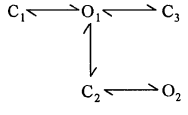
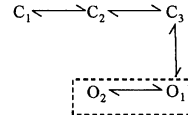
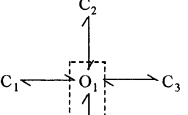
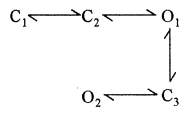
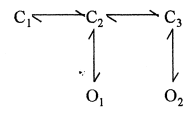
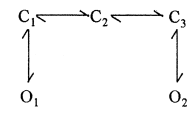
Model 1	Model 2	Model 3
		
Model 4	Model 5	Model 6
		
Model 7	Model 8	Model 9
		
Model 10	Model 11	Model 12
		
Model 13	Model 14	Model 15
		

Table 3. Optimal parameters (s^{-1}) for models having the highest maximum log likelihood values

Patch No.	12170303	12170304	12170305	12170306
Model 1	$ \begin{array}{c} C_1 \xrightarrow{777} C_2 \xrightarrow{4145} O_1 \\ \downarrow 315 \quad \downarrow 464 \quad \downarrow 298 \quad \downarrow 4300 \\ C_3 \quad \quad \quad O_2 \end{array} $	$ \begin{array}{c} C_1 \xrightarrow{1212} C_2 \xrightarrow{4988} O_1 \\ \downarrow 403 \quad \downarrow 1159 \quad \downarrow 416 \quad \downarrow 4624 \\ C_3 \quad \quad \quad O_2 \end{array} $	$ \begin{array}{c} C_1 \xrightarrow{891} C_2 \xrightarrow{4253} O_1 \\ \downarrow 357 \quad \downarrow 959 \quad \downarrow 395 \quad \downarrow 5060 \\ C_3 \quad \quad \quad O_2 \end{array} $	$ \begin{array}{c} C_1 \xrightarrow{810} C_2 \xrightarrow{4647} O_1 \\ \downarrow 397 \quad \downarrow 1013 \quad \downarrow 429 \quad \downarrow 4915 \\ C_3 \quad \quad \quad O_2 \end{array} $
Model 4	$ \begin{array}{c} C_1 \xrightarrow{640} C_2 \xrightarrow{3052} O_1 \\ \downarrow 1931 \quad \downarrow 1715 \quad \downarrow 202 \quad \downarrow 4116 \\ C_3 \quad \quad \quad O_2 \\ \xrightarrow{7213} \xrightarrow{22} \end{array} $	$ \begin{array}{c} C_1 \xrightarrow{577} C_2 \xrightarrow{3470} O_1 \\ \downarrow 1810 \quad \downarrow 1654 \quad \downarrow 256 \quad \downarrow 4545 \\ C_3 \quad \quad \quad O_2 \\ \xrightarrow{8021} \xrightarrow{33} \end{array} $	$ \begin{array}{c} C_1 \xrightarrow{544} C_2 \xrightarrow{2992} O_1 \\ \downarrow 1732 \quad \downarrow 2225 \quad \downarrow 270 \quad \downarrow 4856 \\ C_3 \quad \quad \quad O_2 \\ \xrightarrow{7771} \xrightarrow{32} \end{array} $	$ \begin{array}{c} C_1 \xrightarrow{588} C_2 \xrightarrow{3354} O_1 \\ \downarrow 1962 \quad \downarrow 1830 \quad \downarrow 277 \quad \downarrow 4835 \\ C_3 \quad \quad \quad O_2 \\ \xrightarrow{7820} \xrightarrow{33} \end{array} $
Model 5	$ \begin{array}{c} C_1 \xrightarrow{567} C_2 \xrightarrow{3168} O_1 \\ \downarrow 1731 \quad \downarrow 78 \quad \downarrow 5418 \quad \downarrow 890 \\ O_2 \quad \quad \quad C_3 \\ \xrightarrow{637} \xrightarrow{272} \end{array} $	$ \begin{array}{c} C_1 \xrightarrow{486} C_2 \xrightarrow{3936} O_1 \\ \downarrow 1569 \quad \downarrow 96 \quad \downarrow 5513 \quad \downarrow 862 \\ O_2 \quad \quad \quad C_3 \\ \xrightarrow{857} \xrightarrow{542} \end{array} $	$ \begin{array}{c} C_1 \xrightarrow{500} C_2 \xrightarrow{3116} O_1 \\ \downarrow 1658 \quad \downarrow 111 \quad \downarrow 6672 \quad \downarrow 986 \\ O_2 \quad \quad \quad C_3 \\ \xrightarrow{594} \xrightarrow{219} \end{array} $	$ \begin{array}{c} C_1 \xrightarrow{508} C_2 \xrightarrow{3700} O_1 \\ \downarrow 1718 \quad \downarrow 104 \quad \downarrow 6013 \quad \downarrow 902 \\ O_2 \quad \quad \quad C_3 \\ \xrightarrow{780} \xrightarrow{334} \end{array} $
Model 7	$ \begin{array}{c} C_1 \xrightarrow{5241} O_1 \xrightarrow{773} C_2 \\ \downarrow 941 \quad \downarrow 372 \quad \downarrow 202 \quad \downarrow 4116 \\ O_2 \quad \quad \quad C_3 \\ \xrightarrow{22} \xrightarrow{7221} \end{array} $	$ \begin{array}{c} C_1 \xrightarrow{5490} O_1 \xrightarrow{651} C_2 \\ \downarrow 1004 \quad \downarrow 364 \quad \downarrow 256 \quad \downarrow 4551 \\ O_2 \quad \quad \quad C_3 \\ \xrightarrow{33} \xrightarrow{8048} \end{array} $	$ \begin{array}{c} C_1 \xrightarrow{4928} O_1 \xrightarrow{942} C_2 \\ \downarrow 1284 \quad \downarrow 329 \quad \downarrow 270 \quad \downarrow 4857 \\ O_2 \quad \quad \quad C_3 \\ \xrightarrow{32} \xrightarrow{7786} \end{array} $	$ \begin{array}{c} C_1 \xrightarrow{5547} O_1 \xrightarrow{773} C_2 \\ \downarrow 1059 \quad \downarrow 356 \quad \downarrow 277 \quad \downarrow 4839 \\ O_2 \quad \quad \quad C_3 \\ \xrightarrow{32} \xrightarrow{7840} \end{array} $
Model 8	$ \begin{array}{c} C_3 \quad \quad \quad C_3 \\ \downarrow 1020 \quad \downarrow 6663 \\ C_1 \xrightarrow{376} C_2 \xrightarrow{450} O_1 \\ \downarrow 62 \quad \downarrow 540 \quad \downarrow 323 \quad \downarrow 4250 \\ O_2 \end{array} $	$ \begin{array}{c} C_3 \quad \quad \quad C_3 \\ \downarrow 1090 \quad \downarrow 7069 \\ C_1 \xrightarrow{602} C_2 \xrightarrow{506} O_1 \\ \downarrow 162 \quad \downarrow 513 \quad \downarrow 393 \quad \downarrow 4835 \\ O_2 \end{array} $	$ \begin{array}{c} C_3 \quad \quad \quad C_3 \\ \downarrow 1416 \quad \downarrow 6395 \\ C_1 \xrightarrow{458} C_2 \xrightarrow{406} O_1 \\ \downarrow 80 \quad \downarrow 741 \quad \downarrow 380 \quad \downarrow 4986 \\ O_2 \end{array} $	$ \begin{array}{c} C_3 \quad \quad \quad C_3 \\ \downarrow 668 \quad \downarrow 6333 \\ C_1 \xrightarrow{527} C_2 \xrightarrow{409} O_1 \\ \downarrow 80 \quad \downarrow 356 \quad \downarrow 550 \quad \downarrow 4049 \\ O_2 \end{array} $
Model 11	$ \begin{array}{c} C_3 \quad \quad \quad C_3 \\ \downarrow 1579 \quad \downarrow 4143 \\ C_1 \xrightarrow{362} C_2 \xrightarrow{665} C_3 \\ \downarrow 56 \quad \downarrow 1945 \quad \downarrow 298 \quad \downarrow 4296 \\ O_2 \quad \quad \quad O_1 \end{array} $	$ \begin{array}{c} C_3 \quad \quad \quad C_3 \\ \downarrow 1474 \quad \downarrow 4959 \\ C_1 \xrightarrow{613} C_2 \xrightarrow{672} C_3 \\ \downarrow 159 \quad \downarrow 1830 \quad \downarrow 416 \quad \downarrow 4624 \\ O_2 \quad \quad \quad O_1 \end{array} $	$ \begin{array}{c} C_3 \quad \quad \quad C_3 \\ \downarrow 2084 \quad \downarrow 4220 \\ C_1 \xrightarrow{412} C_2 \xrightarrow{587} C_3 \\ \downarrow 70 \quad \downarrow 1860 \quad \downarrow 394 \quad \downarrow 5060 \\ O_2 \quad \quad \quad O_1 \end{array} $	$ \begin{array}{c} C_3 \quad \quad \quad C_3 \\ \downarrow 1646 \quad \downarrow 4640 \\ C_1 \xrightarrow{526} C_2 \xrightarrow{583} C_3 \\ \downarrow 64 \quad \downarrow 1884 \quad \downarrow 429 \quad \downarrow 4916 \\ O_2 \quad \quad \quad O_1 \end{array} $
Model 12	$ \begin{array}{c} C_2 \quad \quad \quad C_2 \\ \downarrow 993 \quad \downarrow 6320 \\ C_1 \xrightarrow{588} O_1 \xrightarrow{266} C_3 \\ \downarrow 319 \quad \downarrow 275 \quad \downarrow 298 \quad \downarrow 4294 \\ O_2 \end{array} $	$ \begin{array}{c} C_2 \quad \quad \quad C_2 \\ \downarrow 1011 \quad \downarrow 7048 \\ C_1 \xrightarrow{1016} O_1 \xrightarrow{328} C_3 \\ \downarrow 140 \quad \downarrow 316 \quad \downarrow 416 \quad \downarrow 4631 \\ O_2 \end{array} $	$ \begin{array}{c} C_2 \quad \quad \quad C_2 \\ \downarrow 1346 \quad \downarrow 6348 \\ C_1 \xrightarrow{767} O_1 \xrightarrow{507} C_3 \\ \downarrow 233 \quad \downarrow 208 \quad \downarrow 395 \quad \downarrow 5059 \\ O_2 \end{array} $	$ \begin{array}{c} C_2 \quad \quad \quad C_2 \\ \downarrow 1116 \quad \downarrow 6492 \\ C_1 \xrightarrow{364} O_1 \xrightarrow{13} C_3 \\ \downarrow 508 \quad \downarrow 176 \quad \downarrow 430 \quad \downarrow 4917 \\ O_2 \end{array} $

likelihood fitting in model selection (Magleby and Song, 1992; Colquhoun and Hawkes, 1995a; Gil et al., 2001).

Predictions of macroscopic current properties

The four best schemes can be further classified by the number of closed states that must be visited (after full binding) before the

first open state is reached. This property of the reaction scheme predicts distinguishable time courses of the macroscopic current after the fast application of a high concentration of agonists. As shown in Figure 3, if NMDARs must pass through two closed states (e.g., model 8, starting from C_1), the rising phase of macroscopic current should be sigmoidal, whereas if receptors have

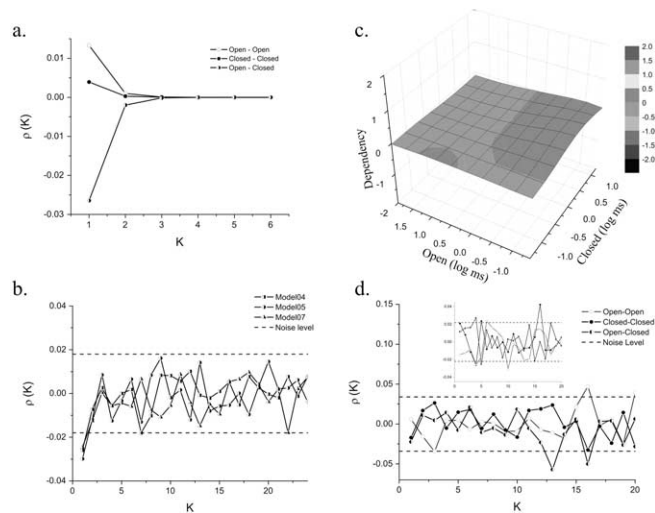


Figure 2. Correlation analyses of NMDAR-idealized single-channel currents, from experimental and simulated currents. *a*, Autocorrelation coefficients of open, closed, and open-closed interval pairs predicted by model 4. *b*, Autocorrelation coefficients of open-closed interval pairs simulated by using models 4, 5, and 7 (total number of events, $n = 11,000$). The dashed horizontal lines are $\pm 2/\sqrt{n}$, which is plus or minus twice the SE of the estimate in the case of white noise. *c*, 2D dependency plot of 7629 intraburst intervals from one outside-out patch. There is no significant dependency between adjacent open and closed intervals. *d*, Autocorrelation coefficients for the open, closed, and open-closed interval pairs from experimental NMDAR current cluster recorded from an outside-out patch ($n = 3274$). Autocorrelation coefficients for the open–open, closed–closed, and open–closed interval pairs from one activation cluster recorded from a cell-attached patch are shown ($n = 9760$) (inset). K , Step size; $\rho(K)$, autocorrelation coefficient.

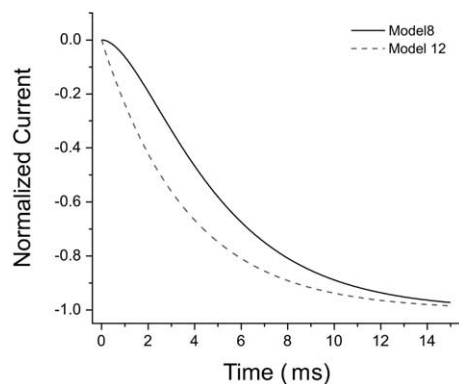


Figure 3. Time course of the macroscopic current predicted by models having different numbers of preopening closed states. The solid line was simulated from model 8 with the assumption that activation starts from C_1 . The dashed line was simulated from model 12 with C_3 as the starting point. The rate constants used for simulation were obtained by globally fitting activation bursts from four patches.

to pass through only one closed state (e.g., model 12), then the rising phase of macroscopic current should be exponential. We sought to discriminate between models by comparing their predictions on the time course of macroscopic currents induced by a step change in the agonist concentration. Note that the models tested here pertain to only the gating reaction; thus, the NMDAR macroscopic currents should exclude ligand binding and desensitization steps.

Saturating concentrations of agonists were applied by a fast perfusion system (solution change $<200 \mu\text{s}$) on outside-out macropatches (Fig. 4*a*). The rising phase of evoked macroscopic current was $<15 \text{ ms}$ (Fig. 4), which is much faster than the time

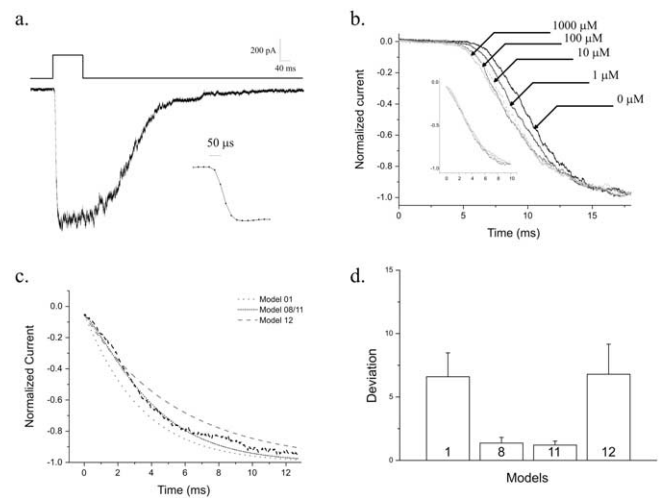


Figure 4. The rising phase of NMDAR macroscopic current evoked by fast application of saturating concentrations of agonists is satisfied by models 8 and 11. *a*, Macroscopic current induced by 1 mM glutamate plus 100 μM glycine applied to an outside-out macropatch (-60 mV). The top trace is the command pulse indicating agonist application. The inset is the open-tip response recorded on the same patch pipette, on expanded scale. *b*, Macroscopic currents after a concentration jump from solutions containing different concentrations of glycine with no glutamate to a solution containing 100 μM glycine and 1 mM glutamate. Alignment of the 5–95% rising phases of the currents is shown (inset). *c*, Comparison of experimental and simulated macroscopic currents. Only the best result from each model was used for comparison. The simulated currents from models 8 and 11 overlap. *d*, Deviations calculated by Equation 7 of predicted currents from experimental current. Models 8 and 11 provide equivalent and superior descriptions of the experimental current. Error bars indicate SE.

constant of NMDAR desensitization ($>100 \text{ ms}$) (Vicini et al., 1998; Villarroel et al., 1998). To confirm that the rising phase was independent of binding steps, a series of jumps from solutions containing various concentrations of glycine to a solution with 1 mM glutamate plus 100 μM glycine was performed (Fig. 4*b*). The rising phases were identical, although the glycine binding steps were different in these jumps. This indicates that that glycine binding did not contribute significantly to the rising phase of NMDAR current at saturating concentration. We could not perform the complementary experiment with glutamate binding, because it is difficult to eliminate background contamination of glycine (Kleckner and Dingledine, 1988). However, the glutamate equilibrium dissociation constant is $\sim 3 \mu\text{M}$, and the association rate constant is $\sim 10^8 \text{ M}^{-1} \cdot \text{s}^{-1}$ (Benveniste and Mayer, 1991*a,b*; Lester and Jahr, 1992; Popescu et al., 2004), which suggests that we could expect full saturation of the binding sites within $\sim 200 \mu\text{s}$. We therefore conclude that the rising phase of the macroscopic current evoked by the fast application of saturating concentrations of agonists can be used to examine the predictions by various models of the gating reaction.

The best predictions by models 1, 8, 11, and 12 are superimposed on normalized NMDAR macroscopic currents in Figure 4*c*. The rising phase of NMDAR current was clearly sigmoidal, in agreement with models 8 and 11 using the rate constants estimated from modeling single-channel interval data. Models 1 and 12 both predicted an exponential rising phase, although in model 12, there were two closed states before the first open state. Overall, the deviations of the predictions by models 8 and 11 were much lower than those of predictions by models 1 and 12 (Fig. 4*d*).

Combining the noncyclic models

After the above three rounds of model selection, we were left with two noncyclic, 3C2O models that provided adequate and equally

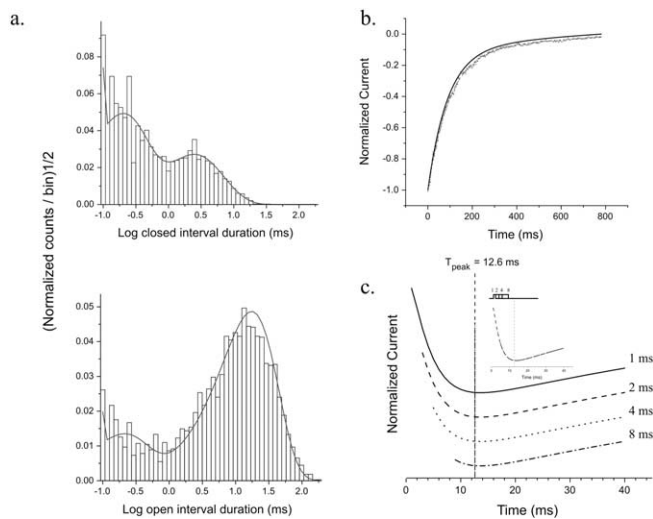
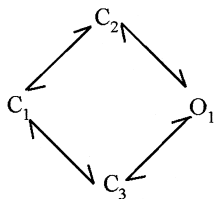


Figure 5. Both microscopic and macroscopic currents are described by model 16. *a*, Histograms of intraburst interval distributions. The solid lines are calculated from the model. *b*, Simulated (solid line) and experimental current decays after a 100 ms pulse of 1 mM glutamate plus 100 μ M glycine. Binding and desensitization states (both connected to C_1) were added to model 16. The dashed line is the fit of experimental current by the sum of two exponentials. *c*, Simulations of the current response to short pulses (1, 2, 4, and 8 ms) of saturating agonists (model 16). The time to peak (T_{peak}) is the same for all pulse durations. Currents are staggered vertically for display purposes. The inset is the superimposed view of these traces.

good descriptions for the activation of NMDAR, at both the microscopic and macroscopic levels. These two models differ in the disposition of closed state C_3 , which is either connected only to O_1 (model 8) or interposed between C_2 and O_1 (model 11). We could not use statistical tests to further distinguish these two models; hence, we combined them into a single cyclic scheme that preserves the key features of both two noncyclic models, namely coupled open states, a single gateway between closed and open aggregates, and multiple preopening closed states.



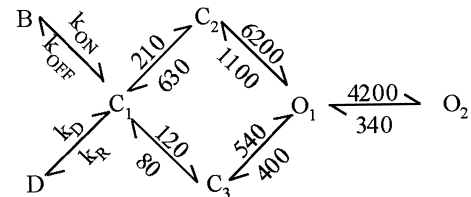
Model 16

Detailed balance was enforced for the cycle in model 16, which had one extra free parameter compared with models 8 and 11.

Figure 5*a* shows that the experimental intracluster closed (top panel) and open (bottom panel) distributions are in good agreement with those predicted by model 16 (continuous lines). In addition, the autocorrelation function of data simulated from this model has the same flat shape as those obtained from NMDAR activation clusters. Model 16 also accurately predicts the time course of macroscopic currents evoked by fast application of agonists when C_1 is the starting state (data not shown). Although neither the LL values obtained from single-channel kinetic modeling nor the deviations of the macroscopic currents from those predicted by the model were significantly improved by the extra free parameter, model 16 is appealing in that it provides an unambiguous gating reaction mechanism for NMDARs.

According to this scheme, there are two alternative conformational pathways in the gating reaction ($C_1C_2O_1$ or $C_1C_3O_1$).

To further evaluate the predictions of model 16, we simulated the decay phase of the macroscopic current after a 100 ms pulse of saturating agonists and compared it with experimentally measured decays. This decay depends on desensitization and ligand dissociation as well as the gating conformational changes (Lester and Jahr, 1992); hence, model 16 alone is insufficient. Using values from previous studies (Benveniste et al., 1990; Lester and Jahr, 1992; Popescu and Auerbach, 2003), we modified model 16 by adding binding and desensitizing steps.

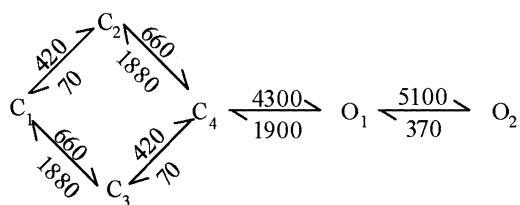


Model 16a

The rate constants are in 1/seconds. B represents all less than fully liganded NMDARs, and D represents fully liganded, desensitized NMDARs. The agonist association and dissociation rate constants are k_{ON} and k_{OFF} , and the entry and recovery rate constants for desensitization are k_{D} and k_{R} . The dissociation rate constant k_{OFF} was chosen as 11.4 s^{-1} ($2 \times k_{\text{OFF_Glu}} + 2 \times k_{\text{OFF_Gly}}$) (Benveniste et al., 1990; Lester and Jahr, 1992), and the desensitization/recovery rate constants were set at $4/1 \text{ s}^{-1}$ (Popescu and Auerbach, 2003). The remaining rate constants were globally fitted using intervals within clusters from four outside-out patches. The desensitized state was connected, in turn, to each state of the scheme, and the best prediction of the decay phase of the NMDAR macroscopic current was obtained when D was connected to C_1 (Fig. 5*c*). The decay of NMDAR macroscopic current evoked by 100 ms pulse of 1 mM glutamate and 100 μ M glycine was fitted by the sum of two exponentials, with time constants (relative amplitudes) of $92.4 \pm 0.27 \text{ ms}$ ($85 \pm 0.3\%$) and $702.2 \pm 46.8 \text{ ms}$ ($15 \pm 0.2\%$), respectively ($n = 3$). The corresponding values for the best match with D connected to C_1 were 88 ms (83%) and 899 ms (17%). The next best match was D connected to C_3 , with values of 87 ms (65%) and 960 ms (35%). The predictions with D connected to states C_2 , O_1 , and O_2 were significantly worse (only a single exponential). This result suggests that NMDAR desensitization occurs mainly from C_1 . Thus, according to model 16, there are three possible fully liganded pathways out of the first nonconducting state: two that lead to opening (after passing through a preopening closed state) and one that leads to desensitization.

We also simulated the response of NMDARs to short pulses of saturating glutamate (1–10 ms) using model 16. The model predicts that the time it takes for the NMDAR current to reach its peak is independent of the length of pulse ($>1 \text{ ms}$). As shown in Figure 5*c*, after the binding of agonists, the time to peak was 12.6 ms for currents evoked by 1, 2, 4, and 8 ms pulses of saturating agonists. This conclusion is in accord with the observation that a pulse of saturating glutamate as short as 0.8 ms produces the maximal response of NMDARs (Lester and Jahr, 1992).

Model 16 shares a structure with the kinetic scheme proposed by Banke and Traynelis for the gating of NMDAR (Banke and Traynelis, 2003). We modified their scheme by adding a second, coupled open state.



Model 17

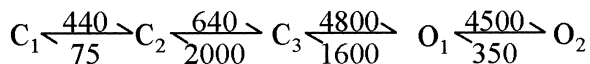
Although model 17 contains four rather than three closed states, the pairs of rate constants on parallel sides of the cycle are constrained to be equal, yielding only eight free parameters. The optimal rate constants are shown in model 17.

In four patches, the average rate constants for the $C_1 \rightleftharpoons C_2$ and $C_2 \rightleftharpoons C_4$ steps in model 17 were essentially the same as the $C_1 \rightleftharpoons C_2$ and $C_2 \rightleftharpoons C_3$ rate constants obtained by using the linear, CCCOO scheme (model 11). Our estimate of the $C_2 \rightleftharpoons C_4$ equilibrium constant (0.35) is >50 times smaller than that reported for NR1/NR2A NMDARs expressed in HEK cells at pH 7.3 (3140/174 $s^{-1} = 18$) (Erreger et al., 2005). Such discrepancy cannot be completely accounted for by the different pHs (8.0 vs 7.3) (Banke et al., 2005) and is perhaps the result of different expression systems.

Discussion

Our objective was to identify kinetic schemes that describe the gating reaction of fully liganded, recombinant NR1a/NR2A NMDARs. In general terms, the statistics-based modeling studies indicate that such a reaction mechanism must (1) contain at least three nonconducting and two conducting states, (2) have only one entry/exit gateway between the nonconducting and conducting aggregates, (3) have coupled conducting states, and (4) have at least two preopening, nonconducting states. We examined the ability of 17 different kinetic schemes to describe both steady-state single-channel currents and macroscopic currents elicited by a jump in agonist concentration. Only two noncyclic models were able to account for these channel behaviors, and these could be combined into a single cyclic scheme.

One of the two noncyclic schemes was a simple linear CCCOO mechanism that had been used previously to predict the NMDAR response to trains of synaptic impulses (Popescu and Auerbach, 2003; Popescu et al., 2004):



Model 11a

The rate constants are in 1/seconds. This reaction mechanism strikes us as being simpler than the alternative, branched model 8, because with it NMDAR gating can be viewed as a straightforward, if sluggish, closed \rightleftharpoons open isomerization ($C_1 \dots \rightleftharpoons \dots O_2$). NMDARs are large proteins in which the binding-site domains and the channel domain are separated by >40 Å (Miyazawa et al., 1999; Furukawa and Gouaux, 2003). Therefore, it is likely that intermediate conformations exist between the stable C_1 and O_2 end states of the reaction. In the linear scheme, some of the intermediate structures that populate the “transition state” of the overall reaction (C_2 , C_3 , and O_1) are sufficiently long-lived to be detected in patch-clamp recordings. In neuromuscular acetylcholine receptor channels, these intermediate conformations are, in general, too brief to be detected as discrete events and can be inferred only by using rate-equilibrium–free-energy relationship

analysis (Auerbach, 2005). A preopening closed–intermediate state has also been observed directly in the glycine receptor channel (Burzomato et al., 2004). With the linear scheme, NMDARs can be thought of as closed-to-open gating devices that have long-lived intermediate states. Accordingly, the effective overall gating rates, which reflect the mean first-passage times between the stable end states of the reaction C_1 and O_2 , are 5.64 ms (forward) and 228 ms (backward). The inverses of these values, 177 s^{-1} and 4.4 s^{-1} , are the appropriate quantities for comparison with studies that model gating as a single, $C \rightleftharpoons O$ step (Erreger et al., 2004).

The lifetimes of the intermediate preopening states C_1 and C_2 are remarkably long (1–2 ms). These states act as “way stations” that serve to slow both the rise and the decay of the synaptic current. Moreover, the lifetime of C_1 is longer than that of a transmitter pulse and allows a single NMDAR to integrate information from multiple synaptic impulses (Popescu and Auerbach, 2003). We speculate that natural selection has operated on the stability of states C_1 and C_2 to enforce these critical pauses in the NMDAR gating reaction.

With two notable exceptions, the conductance and kinetic parameters for NR1a/NR2A NMDARs expressed in oocytes (outside-out patches) or in HEK cells (M-mode; cell-attached patches) (Popescu and Auerbach, 2003), under otherwise-identical experimental conditions, are similar. One important difference is that we observed only one pattern of activity rather than three, as in HEK cells. The reason for this difference is not clear. One possibility is that GFP, coexpressed with the NMDAR subunits only in HEK cells, is responsible. However, the difference might arise from the expression systems themselves. It is known that different expression systems can differ in their translational efficiency, posttranslational modifications such as glycosylation and phosphorylation, subunit or associated-protein assembly, or even lipid environment. For example, it has been reported that there are substantial differences in the kinetics of ClC-2 channels expressed in oocytes versus HEK cells (Thiemann et al., 1992; Jordt and Jentsch, 1997; Park et al., 1998), which can partly be explained by difference in phosphorylation. In another study, it was found that the glycosylation patterns are different between native nicotinic receptors of *Torpedo californica* and those expressed in oocytes (Buller and White, 1990). The multiple activation patterns of NMDARs expressed in HEK cells could be a potential target for modulation, because the open probability of NMDARs in each mode is quite different. If mode switching is a mechanism that can be used to tune the activity of NMDARs in the CNS, it will be interesting to determine whether or not this behavior is a function of the expression system and, if so, which processes govern its occurrence.

The second significant difference between the oocyte and HEK cell kinetic parameters is the kinetics of the $C_1 \rightleftharpoons C_2$ transition. (All other rate constants are within a factor of 2.) In the oocyte experiments, the rate constants for this step were 440/75 s^{-1} (forward/backward; yielding an equilibrium constant of 5.3), whereas in the HEK experiments, these were 150/173 s^{-1} (yielding an equilibrium constant of 0.9, independent of mode). This difference predicts a faster rise and slower decay of the synaptic impulse response using the oocyte values and is thus worth noting, although we have no information regarding the mechanistic basis for this discrepancy.

The cyclic scheme we explored (model 16) has the same general structure as the gating scheme proposed by Banke and Traynelis (2003) for the activation of recombinant NR1/NR2B NMDARs (expressed in HEK), although the methods used to

deduce these two models were quite different. The BT model was based on the observation that partial agonists for glutamate and glycine binding sites alter different components of the interval duration distribution of intracluster closed events, which led to the speculation that, during the gating reaction, the NR2 and NR1 subunits change their conformations independently. In our experiments, model 16 was investigated simply because it incorporated both of the two best noncyclic schemes, and was not based on any assumptions regarding NMDAR structure or gating mechanism. Nevertheless, the similarity of these models, obtained by using completely different approaches, suggests that a dual pathway mechanism for gating is possible. In model 16, C_1 , C_2 , and C_3 act as way stations. The lifetime of C_2 (0.15 ms) is much shorter than that of C_3 (1.6 ms), but C_2 is visited approximately twice as frequently as C_3 within the activation sequence (both forward and backward).

At this stage, we cannot unambiguously associate the kinetic events with particular changes in the conformations of structural domains. Given that glutamate and glycine analogs specifically alter the $C_1 \rightleftharpoons C_2$ and $C_2 \rightleftharpoons C_3$ transitions, it is likely that these events reflect motions of the S1–S2 domains of the NR2 and NR1 subunits (Banke and Traynelis, 2003; Jin et al., 2003). It is uncertain whether or not these preopening isomerizations pertain to conformational changes of entire subunits, because they may also reflect the motions of other domains of the NMDAR (“blocks”) that may or may not be subunit delimited (Chakrapani et al., 2004). We must wait for additional kinetic and other functional analyses of NMDARs that have been perturbed by ligands and mutations before this distinction can be made with confidence.

Although the models we selected adequately account for the data, there are several noteworthy limitations to our study. The currents were not recorded under physiological conditions and therefore the models do not incorporate divalent cation inhibition (Mayer et al., 1984; Nowak et al., 1984) or subconductance levels (Stern et al., 1992, 1994). Ligand binding and desensitization steps were not included in the modeling, although the incorporation of published values for these parameters made accurate predictions with regard to experimental current-decay time courses. Nonetheless, we hope that the information provided by this study will facilitate our future understanding of how NMDARs are used for signal transduction at synapses and how NMDARs operate as protein nanomachines.

References

- Auerbach A (2005) Gating of acetylcholine receptor channels: brownian motion across a broad transition state. *Proc Natl Acad Sci USA* 102:1408–1412.
- Banke TG, Traynelis SF (2003) Activation of NR1/NR2B NMDA receptors. *Nat Neurosci* 6:144–152.
- Banke TG, Dravid SM, Traynelis SF (2005) Protons trap NR1/NR2B NMDA receptors in a nonconducting state. *J Neurosci* 25:42–51.
- Behe P, Stern P, Wyllie DJ, Nassar M, Schoepfer R, Colquhoun D (1995) Determination of NMDA NR1 subunit copy number in recombinant NMDA receptors. *Proc R Soc Lond B Biol Sci* 262:205–213.
- Benveniste M, Mayer ML (1991a) Kinetic analysis of antagonist action at N-methyl-D-aspartic acid receptors. Two binding sites each for glutamate and glycine. *Biophys J* 59:560–573.
- Benveniste M, Mayer ML (1991b) Structure-activity analysis of binding kinetics for NMDA receptor competitive antagonists: the influence of conformational restriction. *Br J Pharmacol* 104:207–221.
- Benveniste M, Clements J, Vyklicky Jr L, Mayer ML (1990) A kinetic analysis of the modulation of N-methyl-D-aspartic acid receptors by glycine in mouse cultured hippocampal neurons. *J Physiol (Lond)* 428:333–357.
- Buller AL, White MM (1990) Altered patterns of N-linked glycosylation of the *Torpedo* acetylcholine receptor expressed in *Xenopus* oocytes. *J Membr Biol* 115:179–189.
- Burzomato V, Beato M, Groot-Kormelink PJ, Colquhoun D, Sivilotti LG (2004) Single-channel behavior of heteromeric $\alpha 1\beta$ glycine receptors: an attempt to detect a conformational change before the channel opens. *J Neurosci* 24:10924–10940.
- Chakrapani S, Bailey TD, Auerbach A (2004) Gating dynamics of the acetylcholine receptor extracellular domain. *J Gen Physiol* 123:341–356.
- Clapham DE, Neher E (1984) Substance P reduces acetylcholine-induced currents in isolated bovine chromaffin cells. *J Physiol (Lond)* 347:255–277.
- Clements JD, Lester RA, Tong G, Jahr CE, Westbrook GL (1992) The time course of glutamate in the synaptic cleft. *Science* 258:1498–1501.
- Colquhoun D, Hawkes AG (1981) On the stochastic properties of single ion channels. *Proc R Soc Lond B Biol Sci* 211:205–235.
- Colquhoun D, Hawkes AG (1982) On the stochastic properties of bursts of single ion channel openings and of clusters of bursts. *Philos Trans R Soc Lond B Biol Sci* 300:1–59.
- Colquhoun D, Hawkes AG (1987) A note on correlations in single ion channel records. *Proc R Soc Lond B Biol Sci* 230:15–52.
- Colquhoun D, Hawkes AG (1995a) The principles of the stochastic interpretation of ion-channel mechanisms. In: *Single-channel recording* (Sakman B, Neher E, eds), pp 397–482. New York: Plenum.
- Colquhoun D, Hawkes AG (1995b) A Q-matrix cookbook: how to write only one program to calculate the single-channel and macroscopic predictions for any kinetic mechanism. In: *Single-channel recording* (Sakman B, Neher E, eds), pp 589–633. New York: Plenum.
- Colquhoun D, Sakmann B (1985) Fast events in single-channel currents activated by acetylcholine and its analogues at the frog muscle end-plate. *J Physiol (Lond)* 369:501–557.
- Dingledine R, Borges K, Bowie D, Traynelis SF (1999) The glutamate receptor ion channels. *Pharmacol Rev* 51:7–61.
- Erreger K, Chen PE, Wyllie DJ, Traynelis SF (2004) Glutamate receptor gating. *Crit Rev Neurobiol* 16:187–224.
- Erreger K, Dravid SM, Banke TG, Wyllie DJ, Traynelis SF (2005) Subunit-specific gating controls rat NR1/NR2A and NR1/NR2B NMDA channel kinetics and synaptic signalling profiles. *J Physiol (Lond)* 563:345–358.
- Fredkin DR, Montal M, Rice JA (1985) Identification of aggregated Markovian models: application to the nicotinic acetylcholine receptor. (LeCam LM, Olshen RA, eds), pp 269–289. Belmont, CA: Wadsworth.
- Furukawa H, Gouaux E (2003) Mechanisms of activation, inhibition and specificity: crystal structures of the NMDA receptor NR1 ligand-binding core. *EMBO J* 22:2873–2885.
- Gibb AJ, Colquhoun D (1991) Glutamate activation of a single NMDA receptor-channel produces a cluster of channel openings. *Proc R Soc Lond B Biol Sci* 243:39–45.
- Gibb AJ, Colquhoun D (1992) Activation of N-methyl-D-aspartate receptors by L-glutamate in cells dissociated from adult rat hippocampus. *J Physiol (Lond)* 456:143–179.
- Gil Z, Magleby KL, Silberberg SD (2001) Two-dimensional kinetic analysis suggests nonsequential gating of mechanosensitive channels in *Xenopus* oocytes. *Biophys J* 81:2082–2099.
- Hamill OP, Marty A, Neher E, Sakmann B, Sigworth FJ (1981) Improved patch-clamp techniques for high-resolution current recording from cells and cell-free membrane patches. *Pflugers Arch* 391:85–100.
- Hollmann M, Heinemann S (1994) Cloned glutamate receptors. *Annu Rev Neurosci* 17:31–108.
- Jin R, Banke TG, Mayer ML, Traynelis SF, Gouaux E (2003) Structural basis for partial agonist action at ionotropic glutamate receptors. *Nat Neurosci* 6:803–810.
- Jonas P (1995) Fast application of agonists to isolated membrane patches. In: *Single-channel recording* (Sakman B, Neher E, eds), pp 231–243. New York: Plenum.
- Jordt SE, Jentsch TJ (1997) Molecular dissection of gating in the ClC-2 chloride channel. *EMBO J* 16:1582–1592.
- Kleckner NW, Dingledine R (1988) Requirement for glycine in activation of NMDA-receptors expressed in *Xenopus* oocytes. *Science* 241:835–837.
- Labarca P, Rice JA, Fredkin DR, Montal M (1985) Kinetic analysis of channel gating. Application to the cholinergic receptor channel and the chloride channel from *Torpedo californica*. *Biophys J* 47:469–478.
- Lester RA, Jahr CE (1992) NMDA channel behavior depends on agonist affinity. *J Neurosci* 12:635–643.
- Magleby KL, Pallotta BS (1983) Burst kinetics of single calcium-activated potassium channels in cultured rat muscle. *J Physiol (Lond)* 344:605–623.

- Magleby KL, Song L (1992) Dependency plots suggest the kinetic structure of ion channels. *Proc R Soc Lond B Biol Sci* 249:133–142.
- Mayer ML, Westbrook GL, Guthrie PB (1984) Voltage-dependent block by Mg^{2+} of NMDA responses in spinal cord neurones. *Nature* 309:261–263.
- Miyazawa A, Fujiyoshi Y, Stowell M, Unwin N (1999) Nicotinic acetylcholine receptor at 4.6 Å resolution: transverse tunnels in the channel wall. *J Mol Biol* 288:765–786.
- Nowak L, Bregestovski P, Ascher P, Herbet A, Prochiantz A (1984) Magnesium gates glutamate-activated channels in mouse central neurones. *Nature* 307:462–465.
- Park K, Arreola J, Begenisich T, Melvin JE (1998) Comparison of voltage-activated Cl⁻ channels in rat parotid acinar cells with ClC-2 in a mammalian expression system. *J Membr Biol* 163:87–95.
- Patlak JB (1988) Sodium channel subconductance levels measured with a new variance-mean analysis. *J Gen Physiol* 92:413–430.
- Popescu G, Auerbach A (2003) Modal gating of NMDA receptors and the shape of their synaptic response. *Nat Neurosci* 6:476–483.
- Popescu G, Auerbach A (2004) The NMDA receptor gating machine: lessons from single channels. *Neuroscientist* 10:192–198.
- Popescu G, Robert A, Howe JR, Auerbach A (2004) Reaction mechanism determines NMDA receptor response to repetitive stimulation. *Nature* 430:790–793.
- Premkumar LS, Auerbach A (1996) Identification of a high affinity divalent cation binding site near the entrance of the NMDA receptor channel. *Neuron* 16:869–880.
- Qin F (2004) Restoration of single-channel currents using the segmental k-means method based on hidden Markov modeling. *Biophys J* 86:1488–1501.
- Qin F, Auerbach A, Sachs F (1996) Estimating single-channel kinetic parameters from idealized patch-clamp data containing missed events. *Biophys J* 70:264–280.
- Rosenmund C, Stern-Bach Y, Stevens CF (1998) The tetrameric structure of a glutamate receptor channel. *Science* 280:1596–1599.
- Sakmann B, Patlak J, Neher E (1980) Single acetylcholine-activated channels show burst-kinetics in presence of desensitizing concentrations of agonist. *Nature* 286:71–73.
- Sigworth FJ, Sine SM (1987) Data transformations for improved display and fitting of single-channel dwell time histograms. *Biophys J* 52:1047–1054.
- Song L, Magleby KL (1994) Testing for microscopic reversibility in the gating of maxi K⁺ channels using two-dimensional dwell-time distributions. *Biophys J* 67:91–104.
- Stern P, Behe P, Schoepfer R, Colquhoun D (1992) Single-channel conductances of NMDA receptors expressed from cloned cDNAs: comparison with native receptors. *Proc R Soc Lond B Biol Sci* 250:271–277.
- Stern P, Cik M, Colquhoun D, Stephenson FA (1994) Single channel properties of cloned NMDA receptors in a human cell line: comparison with results from *Xenopus* oocytes. *J Physiol (Lond)* 476:391–397.
- Sun Y, Olson R, Horning M, Armstrong N, Mayer M, Gouaux E (2002) Mechanism of glutamate receptor desensitization. *Nature* 417:245–253.
- Thiemann A, Grunder S, Pusch M, Jentsch TJ (1992) A chloride channel widely expressed in epithelial and non-epithelial cells. *Nature* 356:57–60.
- Vicini S, Wang JF, Li JH, Zhu WJ, Wang YH, Luo JH, Wolfe BB, Grayson DR (1998) Functional and pharmacological differences between recombinant N-methyl-D-aspartate receptors. *J Neurophysiol* 79:555–566.
- Villarroel A, Regalado MP, Lerma J (1998) Glycine-independent NMDA receptor desensitization: localization of structural determinants. *Neuron* 20:329–339.
- Wollmuth LP, Sakmann B (1998) Different mechanisms of Ca²⁺ transport in NMDA and Ca²⁺-permeable AMPA glutamate receptor channels. *J Gen Physiol* 112:623–636.
- Wollmuth LP, Kuner T, Sakmann B (1998) Intracellular Mg²⁺ interacts with structural determinants of the narrow constriction contributed by the NR1-subunit in the NMDA receptor channel. *J Physiol (Lond)* 506:33–52.
- Wyllie DJ, Behe P, Colquhoun D (1998) Single-channel activations and concentration jumps: comparison of recombinant NR1a/NR2A and NR1a/NR2D NMDA receptors. *J Physiol (Lond)* 510:1–18.